Modelling Physical Human-Robot Interface with Different Users, Cuffs, and Strapping Pressures: A Case Study

Mingrui Sun[1], Tomislav Baček[1*], Dana Kulić[2], Jennifer McGinley[3], Denny Oetomo[1], Ying Tan[1]

***Abstract*— Assisting persons during physical therapy or augmenting their performance often requires precise delivery of an intervention. Robotic devices are perfectly placed to do so, but their intervention highly depends on the physical human-robot connection. The inherent compliance in the connection leads to delays and losses in bi-directional power transmission and can lead to human-robot joint axes misalignment. This is often neglected in the literature by assuming a rigid connection and has a negative impact on the intervention's effectiveness and robustness. This paper presents the preliminary results of a study that aims to close that gap. The study investigates what model forms and parameters best capture human-robot connection dynamics across different persons, connection designs (cuffs), and cuff strapping pressures. The results show that the linear spring-damper model is the best compromise, but its parameters must be adjusted for each individual and different conditions separately.**

***Index Terms*— physical human-robot interaction, modelling**

I. Introduction

Robot-assisted intervention is emerging as a promising approach for augmenting human performance or recovering lost abilities. A crucial component in this approach is the physical connection between the human and the robot, called the physical human-robot interface (pHRI). Traditionally considered a rigid component, pHRI has been gaining a lot of interest due to research demonstrating significant losses coming from human non-homogenous soft tissues and soft elements (e.g., straps, cuffs) that make pHRI. This paper contributes to the topic by investigating different model forms and model coefficients that best capture human-robot connection dynamics.

The compliant (non-rigid) parts of pHRI, including human soft tissues and robotic cuffs, although help absorb impact and tolerate misalignments, negatively affect robot-human power transmission, causing delays and significant losses. The reshaping and delays between the assistance robots initiate and the human users receive were quantified as a 55% power loss in the loading phase and partial return in the unloading phase in the case of an angle exosuit device [1]. Similarly, compliant pHRI can also lead to human-robot joint misalignment. For example, the cuff migration with respect to the skin can exceed 4 cm [2] during robot-assisted movements due to skin stretching and cuff sliding [3]. Combined with the human-robot kinematic (joint) incompatibility, the difference in angular movement can be larger than 6° [4].

The losses in pHRI can be accounted for using (mechanistic) models that capture the mechanical properties of compliance in humans and robots. Modeling human-robot systems is not a new approach, as numerous studies have exploited this pathway to optimize the metabolic cost of walking [5], improve athletic performance [6], and evaluate innovative control algorithms for specific gait disorder treatments [7], [8]. Other examples include evaluating pHRI designs that minimize discomfort and misalignment [9], [10] and actuator design optimization [11], [12]. What is missing in all these applications is a realistic representation of the pHRI behavior (models). The studies regularly assume rigid connection and lossless force transmission [5]–[8], [12] or use simple pHRI models without well-informed pHRI parameters [13], [14]. This is a bottleneck in robot-assisted interventions, as poorly understood and modeled pHRI has major negative impacts on the effectiveness, efficiency, and robustness of the interaction.

A limited number of studies on pHRI modelling can already be found in the literature. For example, Schiele [15] proposed a spring-damper model in the tangential direction to the skin, subsequently extended to a spring-damper-attitude model with the inclusion of joint angle in the same direction [2]. More recently, Shafiei and Behzadipour [9] included the normal direction to the skin and rotational directions in a linear spring model but without evaluating the model fitting quality. A common limitation across these studies is the model evaluation using a single strapping pressure, a single cuff, and a small sample. Such restricted testing conditions are major limitations in the interpretation of the results, more so as studies have shown that pHRI model parameters may be affected by factors such as interface geometry, compliance, and the cuff position on the leg segment [16], [17]. This is particularly true in the normal direction to the skin, where the force from the exoskeleton is primarily transmitted to the human limb.

In this study, we present preliminary results of the quantitative evaluation of pHRI that considers the effects of the cuff geometry, cuff strapping pressure, and individual differences. In particular, we show how pHRI model form and parameters vary across four healthy participants tested with two cuff designs and two strapping pressures. The results validate using a linear spring-damper model across all six degrees of freedom (three forces and moments) but demonstrate the need for user and interface-specific model parameters.

This work was funded by the Australian Research Council, Project scheme (DP190100916).

*The corresponding author: tomislav.bacek@unimelb.edu.au

[1] M.Sun, T.Baček, D.Oetomo and Y.Tan are with the Faculty of Engineering and Information Technology, The University of Melbourne, VIC, Australia.

[2] D. Kulić is with the Faculty of Engineering, Monash University, VIC, Australia.

[3] J.McGinley is with the Faculty of Medicine, Dentistry and Health Sciences, The University of Melbourne, VIC, Australia.

II. Methodology

A. Participants

Four healthy young male adults (28±2 years, body mass 83.8 ±19.9 kg, height 182.5±7.0 m, thigh circumference 54.2±8.5 cm) participated in the study. No participant had any physical or biomechanical issues that would affect their participation. The study was approved by the ethics committee of The University of Melbourne (2022-24842-31294-2).

B. Experimental Setup

The investigation of pHRI modeling design and parameters is carried out in a static setup in a biomechanics lab. The setup consists of a chair for participants to sit on, a base frame, a cuff strapped around the person's right leg, an *excitation* frame used to manually generate cuff movement in space, and a six-degree-of-freedom force/torque sensor connecting the cuff and the excitation frame (Fig. 1.a). The undesired lateral leg movement is minimized by two adjustable base frame extrusions, one on each side of the right knee. The chair height and position are also adjustable to ensure the participant's thigh is always parallel to the ground and the thigh-shank linkage forms a perpendicular angle.

The cuffs used in the study include one 3D-printed cuff in PLA plastic (Cuff_A, Fig. 1.b) and one taken off the commercially available Fourier X2 exoskeleton (Fourier Intelligence, Shangai, China; Cuff_B, Fig. 1.c). The Cuff_A is designed based on a 3D scan of a young healthy adult and adapted in size to different participants. The cuff is secured by two wide BOA straps on the distal ends of the cuff. The Cuff_B has a hard C-shaped shell and soft padding with two adjustable straps that wrap around the leg. Both cuffs are instrumented with four pressure sensors (Flexiforce, Tekscan) between the hard shell and padding to measure strapping pressure.

A sturdy aluminum (i.e., *excitation*) frame is used to generate desired movements of the cuff in 3D space, including the three translations and rotations. The frame and cuff are connected by a 6-axis force/torque sensor (Robotous, Korea), easily attachable to allow quick change of cuffs between tests. The sensor measures the interaction wrench (force and torque) at 100Hz, the same frequency as the marker-based Vicon motion capture system (Vicon, UK). The markers define the relative position and orientation of the leg and frame (i.e., cuff). Three functional and one auxiliary markers are placed on the thigh, the former including markers placed on the lateral condyle, medial epicondyle, and greater trochanter of the femur. The cuff's position and orientation are defined by four markers on the excitation frame, forming a rigid body.

The frame also houses a 3-axis accelerometer, placed close to one of the excitation frame markers. The data from the four pressure sensors, force/torque sensor, and accelerometer are recorded by an embedded computer running Linux OS (Jetson TX2, NVIDIA, USA). The data from Vicon and Jetson are recorded separately and synchronized by matching the acceleration of the marker and the accelerometer [18].

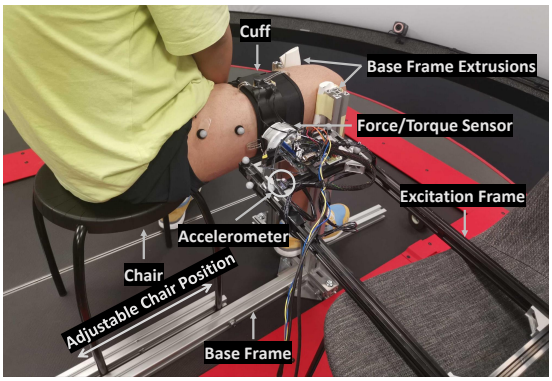

(a) Experimental setup

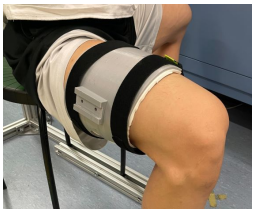

(b) Cuff_A

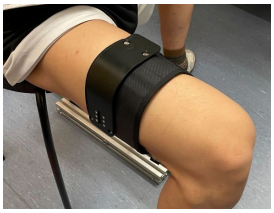

(c) Cuff_B

Fig. 1: The experimental setup. (a) The setup consists of a chair with an adjustable position/height, a base frame with two extrusions, an excitation frame, a cuff, retroreflective markers, a force-torque 6 DoF sensor, and accelerometer. (b) In-house 3D-printed cuff. (c) Commercially-available cuff.

C. Experimental Protocol

The main objective of the experiment is to examine the interaction force and relative displacement under various pHRI configurations with several subjects. The configurations include four combinations of the two cuffs and two strapping pressures that are applied to four healthy young adult subjects.

The experiment is divided into two sessions taking place on separate days (see Fig. 2). Session 1 aims to identify the two strapping pressures for the tests, while the second serves as a data collection day. During Session 1, the subjects are instructed to sit on a chair with the distal end of the thigh fixed (by frame extrusion) while the two cuffs are donned by a physiotherapist (PT). The pressure between the cuff and the soft tissue is measured using four force-resistive sensors (FSR) placed at each corner, providing a level of tightness our PT would apply in clinical practice. The obtained pressure (an average of four measured values) represents the baseline per cuff per subject and is denoted as *Loose* (30kPa). The baseline pressure is averaged across subjects to get a single value per cuff, which is then increased by 20% to form a second level for comparison (denoted *Tight*).

In Session 2, the subjects are instructed to sit in the same position as in Session 1 and keep their lower limb muscles relaxed during the experiment. The four pHRI configurations include *Cuff_A Tight*, *Cuff_A Loose*, *Cuff_B Tight*, and *Cuff_B Loose*. In each configuration (i.e., bout), the investigator manually applies a pre-defined set of three translations and

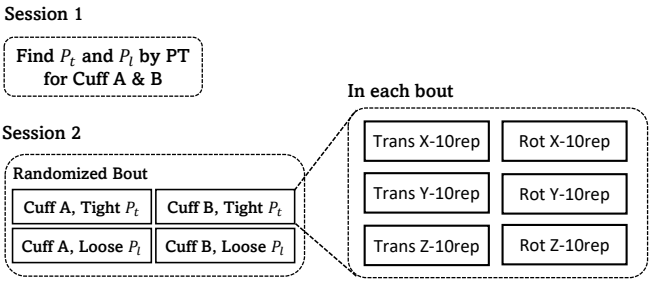

Fig. 2: Experimental protocol. Session 1 serves to determine loose P_l and tight P_t strapping pressures per cuff. The data are collected in Session 2 across four configurations (bouts). In each bout, three translational and rotational cuff movements are manually applied in a pre-defined order, with each movement repeated 10 times before moving on to the next one.

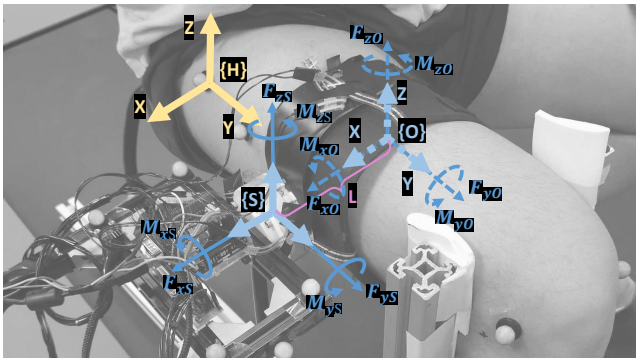

Fig. 3: Coordinate frames and force/moment definitions. The axes of all three frames (human H, sensor S, and orthosis O) follow the same convention: the x-axis is perpendicular to the leg in the medio-lateral direction, the y-axis is defined along the thigh, and the z-axis coincides with the vertical line.

three rotations, always in the same order. The movements are applied sequentially, repeating 10 times each at a 1 Hz frequency (guided by a metronome), followed by a 1-sec pause before moving on to the next movement. The order of the four bouts is randomized for each subject.

D. Data Processing

1) Relative displacement: The relative displacement consists of three translational (ΔT) and three rotational (ΔR) degrees of freedom (DoFs) defined between the human and the excitation frame. The human frame H is attached to the thigh joint, assumed to coincide with the hip marker. The excitation frame origin O is set to coincide with the force sensor origin, subsequently translated along the x axis to sit on the thigh's central axis (the center of the applied rotational movements). Fig. 3 shows all the relevant frames and axes definitions.

The translation is defined as displacement between the origins of the two coordinate frames, and rotation by the Tait–Bryan angles (yaw, pitch, roll) between the two coordinate frames. Before the recording starts, the excitation frame is leveled parallel to the ground and this position is treated as a bias to zero-level the rest of the data. The translational and rotational velocities are calculated by differentiating corresponding displacements and filtered with a zero-phase Butterworth filter (8 Hz cut-off frequency).

2) Interaction wrench correction: The interaction wrench of interest is that with respect to frame O, as this is the origin where the relative displacement is defined. However, the force F and torque M sensor measurements need to be corrected (transformed) from the sensor's origin S to origin O. The following corrections are used:

$$F_{i,O} = F_{i,S} \tag{1}$$
$$M_{x,O} = M_{x,S} \tag{2}$$
$$M_{y,O} = M_{y,S} + L \cdot F_{z,S} \tag{3}$$
$$M_{z,O} = M_{z,S} + L \cdot F_{y,S} \tag{4}$$

where L is the S-O origin distance and $i \in \{x, y, z\}$. The recorded interaction force and torque are zero-leveled by averaging the readings during the first second of recording when the excitation frame is held still in its leveled position.

E. Model Structure

The purpose of the model is to describe the force-displacement relationship in the three translational, as well as the moment-displacement relationship in the three rotational directions. The model comprises six functions that characterize each DoF independently, i.e., without accounting for coupling effects, and is defined as follows:

$$F_i = f_i(\Delta T_i, \Delta \dot{T}_i) \tag{5}$$
$$M_i = g_i(\Delta R_i, \Delta \dot{R}_i) \tag{6}$$

Here, ΔT_i is the translation in direction i, and ΔR_i is the rotation about direction i, where $i \in \{x, y, z\}$. In other words, the model considers both spring (S) and damper (D) terms in trying to capture pHRI dynamics.

Various function forms $h()$ for f_i and g_i are tested. The tested functions mapping force/torque to displacement and velocity include both linear and nonlinear forms, determined by order of displacement and velocity terms used. We also include models with linear and piece-wise linear coefficients to account for the potential heterogeneous directional behavior. The function composition is denoted as h_{P_j,S_r,D_z}, with the following meaning of each element: P refers to the linear-coefficient (j=0) and piece-wise linear-coefficient (j=1) function; S and D denote displacement and velocity terms; and r and z subscripts denote the corresponding order of each term, all respectively. The mathematical formulation of the linear-coefficients function is given as:

$$h_{P_0,S_r,D_z}(x, \dot{x}) = \sum_{n=0}^{r} k_n x^n + \sum_{m=0}^{z} b_m \dot{x}^m, \tag{7}$$

and of the piece-wise linear-coefficients function as:

$$h_{P_1,S_r,D_z}(x,\dot{x}) = \sum_{n=0}^{r} p_n x^n + \sum_{m=0}^{z} q_m \dot{x}^m, \qquad (8)$$

where

$$p_n = \begin{cases} k_{n+}, & x \geq 0 \\ k_{n-}, & x < 0 \end{cases} \qquad q_m = \begin{cases} b_{m+}, & \dot{x} \geq 0 \\ b_{m-}, & \dot{x} < 0. \end{cases}$$

For this study, we consider displacement and velocity terms up to the third order ($r, z \leq 3$). This, combined with piece-wise and non-piece-wise options, results in a total of 32 function compositions of f_i and g_i tested.

F. Model Fitting

The scheme of model fitting is depicted in Fig. 4. For a given subject-pHRI configuration (columns, four per cuff-pressure combination) and a given function composition (rows, 1-32), the model is fitted (each *Fit* block) separately in the six directions using the data collected in the corresponding direction. For example, to fit a function in the *x* direction, only data collected during the translational movement in the same direction are used. The composition (i.e., order) of all functions ($f_x, f_y, f_z, g_x, g_y, g_z$) is kept the same in a given fit.

To ensure fair comparison across all tests, force and moment data are capped at $\pm 80N$ and $\pm 10Nm$, respectively, representing the minimum values achieved in all tests. The data are subsequently separated into training:test set as 70%:30%. The model is fitted using the least squares method and the fit quality evaluated by the coefficient of determination (R^2) and variance across all testing conditions.

III. Results

The results section shows the effects model composition (the order of S and D terms), linearity (piece-wise and non-piece-wise), and the amplitude of model coefficients (k and b) have on capturing the actual pHRI dynamics. To begin with, Fig. 5 illustrates the independent contribution to fitting quality from each (S and D) term in f_i and g_i. This is done up to the fifth order (e.g., kx,..., kx^5) using the $y = cx + d$ regression model. As results show, a linear spring behavior explains pHRI to high levels of accuracy (R^2=0.941 on average) in all six DoFs. Contrary to this, damping terms make a very small contribution, with an average coefficient of determination R^2=0.029). Higher power coefficients in both x and $\dot{x}$ are weaker predictors of the dependent variable, with the contribution dependent mostly on the pHRI configuration (and less on the DoFs).

Fig. 6 shows a fitting quality of f_i and g_i compositions made of S and D terms up to the third order (as per Fig. 5 outcomes). Datapoints are averaged across all 16 conditions, generated by combining the order of D term (four shapes) and order of S term (three colors). Starting from a linear spring model (green circle, Sx and no D), the biggest improvement across all S-D combinations comes from adding a linear damper ($S1D1$). Further increasing model complexity comes with diminishing returns, leaving linear spring – linear damper model as the best possible trade-off. Interestingly, increasing model complexity decreases NMRSE (normalized root mean square error) variance in all DoFs except x rotation.

The results so far considered fixed k and b across both positive and negative directions. Fig. 7 shows how separating the two directions (i.e., piece-wise linearity, see (8)) affects model fitting quality. Clearly, the change is marginal in either of the six DoFs, albeit it slightly improves the accuracy in all. Compared to an average decrease in NRMSE of 0.0075 when spring or damper order is increased to 3, respectively (each doubling the number of parameters in the model), an average decrease of 0.0039 coming from piece-wise linearity

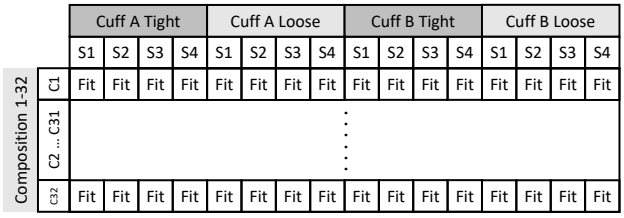

Fig. 4: The scheme of the model fitting procedure. For each subject (4), cuff (2), and strapping pressure (2) combinations (16 total, columns), 32 different models (rows) are fitted corresponding to different orders of translational and rotational displacement and velocity.

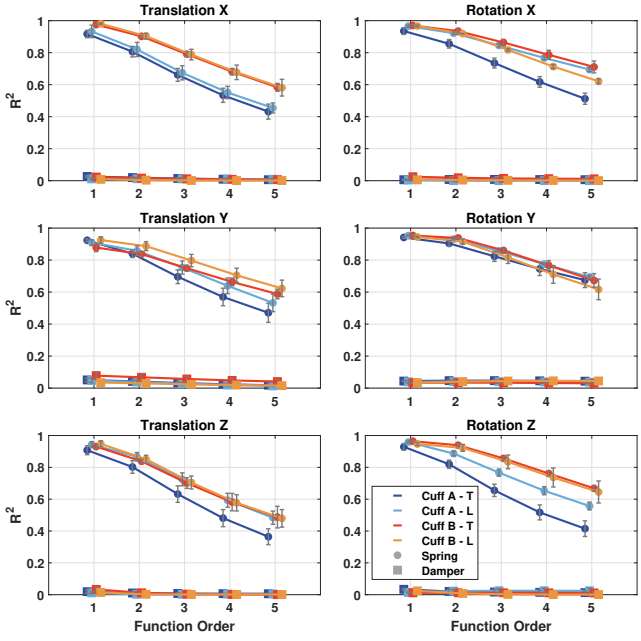

Fig. 5: The significance of the order of Spring and Damper terms in the pHRI model. The four pHRI configurations are evaluated separately, with *T* and *L* denoting *Tight* and *Loose* strapping pressures. Where overlapping, the data points for that function order are separated horizontally for clear presentation.

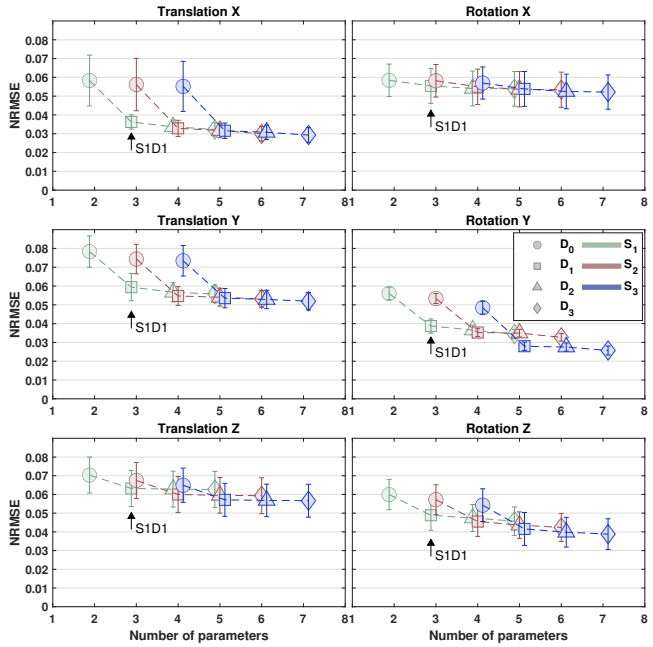

Fig. 6: Effects of model compositions on fitting quality. Three colours and four shapes denote different orders of S and D terms, respectively. Datapoints are an average of 4 subjects, 2 cuffs, and 2 strapping pressures (16 conditions). For a given shape (e.g., circle, D_0), a change in colour represents a change in the order of S terms. For a given colour (e.g., blue, S_3), a change in shape represents a change in the order of D terms. Left to right increases the model complexity.

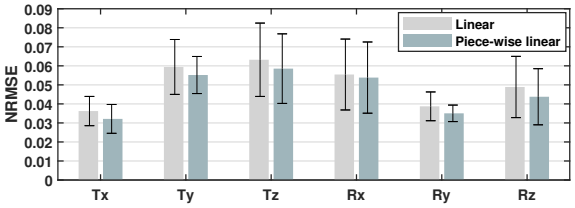

Fig. 7: The comparison of linear and piece-wise linear model coefficients on fitting quality. Bars represent the mean and whiskers standard deviation of the linear spring-linear damper model ($S1D1$) across all pHRI configurations and subjects.

is not sufficient to justify the added complexity.

Variations in pHRI stiffness amplitude for the different cuff-strapping pressure configurations and in all six DoFs are shown in Fig. 8. The stiffness values represent k_1 in a linear spring – linear damper model ($S1D1$ in (7)), as earlier results demonstrated this to be a model of high fitting quality and low variance across conditions (i.e., this model reflects the true stiffness in pHRI dynamics). Both cuff type and strapping pressure affect the estimated pHRI stiffness across all participants. The biggest changes include an increase of about 52% and 25% when going from *loose* to *tight* in Cuff_A and Cuff_B (y translation) and an increase of about

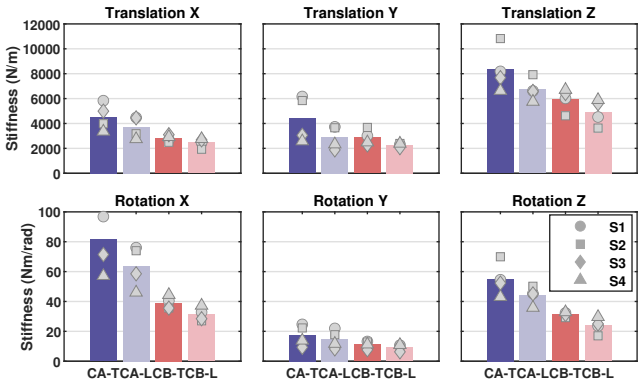

Fig. 8: Variation in estimated pHRI stiffness for different testing conditions. Bars represent mean values, with individual values (per participant) given as data points. Different cuff-strapping pressure combinations are colour-coded. Notice the same y-axis limits per row.

TABLE I: The range of pHRI stiffness amplitudes per DoF.

Stiffness	Tx	Ty	Tz	Rx	Ry	Rz
Max	5654	6165	10835	99.6	24.6	71.8
Min	1926	188.2	3655.97	28.4	6.29	17.1

The units: N/m for Tx, Ty, Tz, and Nm/rad for Rx, Ry, Rz.

102% and 112% when changing from Cuff_A→Cuff_B for *loose* and *tight* configurations (x rotation), all respectively. The range of pHRI stiffness values across the subjects and cuffs, separated into DoFs, are given in Table. I.

IV. Discussion

This study investigated the effects of cuff design, strapping pressure, and individual differences (in leg composition) on the complexity of and coefficients in pHRI modelling. Capturing the inherent compliance in the human-robot connection model is gaining momentum, but little progress has been made. The results presented herein are an important step in closing that gap and growing our understanding of interaction dynamics.

The strapping pressure identified by a PT in Session 1 following clinical guidelines in securing a cuff was much higher for Cuff_A. This is due to a customised design and larger contact surface that allow comfort at a tighter fit, an outcome also predicted by the PT. Higher strapping pressure resulted in a significant drop in higher order k term contributions for Cuff_A (Fig. 5), indicating stronger linearity in the data. This aligns with polynomial force-displacement patterns found in [19], [20], where human tissue was characterised using a pen-like device of a small pressure area.

A linear spring-damper pHRI model, often used in the literature [2], [15], [17] due to its intuitiveness, emerged as a good trade-off between complexity and quality in this work as well (Fig. 6). Where our work contributes is a quantification of the S and D terms' relevance in all six DoFs, up to the fifth order, providing much-needed insights into multi-dimensional human-robot interaction dynamics.

Results indicate high statistical significance of the S and low of the D term in model accuracy (Fig. 5), which meant we could only provide a range of k values with high confidence. Further examining the effects of k terms by using a piece-wise linear approach ((8) and Fig. 7) shows that the pHRI has largely uniform stiffness in positive and negative directions in all 6 DoFs. This is specific to the human thigh due to its large muscle concentration and is unlikely to be found on the shank.

The identified stiffness range differs across the two cuffs (Fig. 8), with the lower one in Cuff_B comparable to the literature [9]. The biggest relative drop in stiffness is seen in x rotation, a DoF where robotic assistance is provided (and thus the most important DoF), with the average drop across all DoFs in going from Cuff_A to Cuff_B 35.5%($\pm$12.3%) for *Tight* and 32.5%($\pm$13.7%) for *Loose* case. The drop was smaller for each cuff when changing from *Tight* to *Loose*, averaging 20.9%($\pm$7.9%) for Cuff_A and 18.2%($\pm$6%) for Cuff_B, suggesting that cuff design has a higher impact than a strapping pressure. Since lower stiffness acts as a bigger energy sink in transmitting robotic assistance to humans, these numbers illustrate the importance of a good fit, a result of custom cuff designs and adequate strapping pressure.

The variations in pHRI stiffness properties with changes in cuff design, strapping pressure, and between individuals demonstrate the need to approach the design of pHRI considering the needs and biomechanical features of each individual. As a step further, the pHRI stiffness can potentially be exploited as a compliant element in compliant actuators, leading to a more compact and user-tailored exoskeleton design. This will require a more elaborate experimental design to characterise pHRI across more conditions and participants, including standing and (assisted) walking. We aim to address this in the coming work, thus overcoming the limited amplitude and velocity of the excitation signal, as well as the small sample, the main limitations of this work.

V. Conclusion

In this work, we investigated the relationship between the relative displacement and interaction force at pHRI in a sitting position. The outcomes of testing pHRI models of different complexity show that the linear spring-damper model captures most of the observed dynamics, equally well in all six DoFs. However, the identified variations in pHRI stiffness with changes in cuff designs, strapping pressure, and among individuals demonstrate the opportunity to include and personalise pHRI models, and corresponding controllers for each individual, to compensate for losses in transmission, leading to more effective design of wearable robots.

References

[1] Yandell, M. B. *et al.*"Physical interface dynamics alter how robotic exosuits augment human movement: Implications for optimizing wearable assistive devices," *Journal of NeuroEngineering and Rehabilitation*, vol. 14, no. 1, p. 40, Dec. 2017.

[2] Akiyama, Y., Yamada, Y. & Okamoto, S."Interaction forces beneath cuffs of physical assistant robots and their motion-based estimation," *Advanced Robotics*, vol. 29, no. 20, pp. 1315–1329, Oct. 2015.

[3] Akiyama, Y. *et al.*"Measurement of Contact Behavior Including Slippage of Cuff When Using Wearable Physical Assistant Robot," *IEEE Transactions on Neural Systems and Rehabilitation Engineering*, vol. 24, no. 7, pp. 784–793, Jul. 2016.

[4] Zanotto, D. *et al.*"Knee Joint Misalignment in Exoskeletons for the Lower Extremities: Effects on User's Gait," *IEEE Transactions on Robotics*, vol. 31, no. 4, pp. 978–987, Aug. 2015.

[5] Dembia, C. L. *et al.*"Simulating ideal assistive devices to reduce the metabolic cost of walking with heavy loads," *PLOS ONE*, vol. 12, no. 7, p. e0180320, Jul. 2017.

[6] Ostraich, B. & Riemer, R."Design of a Multi-Joint Passive Exoskeleton for Vertical Jumping Using Optimal Control," *IEEE Transactions on Neural Systems and Rehabilitation Engineering*, vol. 30, pp. 2815–2823, 2022.

[7] Khamar, M., Edrisi, M. & Forghany, S."Designing a robust controller for a lower limb exoskeleton to treat an individual with crouch gait pattern in the presence of actuator saturation," *ISA Transactions*, vol. 126, pp. 513–532, Jul. 2022.

[8] Mosconi, D. *et al.*"Design and validation of a human-exoskeleton model for evaluating interaction controls applied to rehabilitation robotics," in *2020 8th IEEE RAS/EMBS International Conference for Biomedical Robotics and Biomechatronics (BioRob)*. New York City, NY, USA: IEEE, Nov. 2020, pp. 629–634.

[9] Shafiei, M. & Behzadipour, S."The Effects of the Connection Stiffness of Robotic Exoskeletons on the Gait Quality and Comfort," *Journal of Mechanisms and Robotics*, vol. 12, no. 1, p. 011007, Feb. 2020.

[10] Sánchez-Villamañán, M. C., Torricelli, D. & Pons, J. L."Modeling Human-Exoskeleton Interaction: Preliminary Results," in *Wearable Robotics: Challenges and Trends*," Carrozza, M. C., Micera, S. & Pons, J. L., Eds. Cham: Springer International Publishing, 2019, vol. 22, pp. 137–141.

[11] Shiqian Wang, Meijneke, C. & van der Kooij, H."Modeling, design, and optimization of Mindwalker series elastic joint," in *2013 IEEE 13th International Conference on Rehabilitation Robotics (ICORR)*. Seattle, WA: IEEE, Jun. 2013, pp. 1–8.

[12] Verstraten, T. *et al.*"Optimizing the power and energy consumption of powered prosthetic ankles with series and parallel elasticity," *Mechanism and Machine Theory*, vol. 116, pp. 419–432, Oct. 2017.

[13] Serrancoli, G. *et al.*"Subject-Exoskeleton Contact Model Calibration Leads to Accurate Interaction Force Predictions," *IEEE Transactions on Neural Systems and Rehabilitation Engineering*, vol. 27, no. 8, pp. 1597–1605, Aug. 2019.

[14] Silva, P. C., Silva, M. T. & Martins, J. M."Evaluation of the contact forces developed in the lower limb/orthosis interface for comfort design," *Multibody System Dynamics*, vol. 24, no. 3, pp. 367–388, Oct. 2010.

[15] Schiele, A."An explicit model to predict and interpret constraint force creation in pHRI with exoskeletons," in *2008 IEEE International Conference on Robotics and Automation*. Pasadena, CA, USA: IEEE, May 2008, pp. 1324–1330.

[16] Levesque, L. & Doumit, M."Study of human-machine physical interface for wearable mobility assist devices," *Medical Engineering & Physics*, vol. 80, pp. 33–43, Jun. 2020.

[17] Langlois, K. *et al.*"Investigating the Effects of Strapping Pressure on Human-Robot Interface Dynamics Using a Soft Robotic Cuff," *IEEE Transactions on Medical Robotics and Bionics*, vol. 3, no. 1, pp. 146–155, Feb. 2021.

[18] Schulte, R. V. *et al.*"Synchronization of wearable motion capture and EMG measurement systems," in *2022 International Conference on Rehabilitation Robotics (ICORR)*. Rotterdam, Netherlands: IEEE, Jul. 2022, pp. 1–6.

[19] Aso, M. *et al.*"Evaluation of the mechanical characteristics of human thighs for developing complex dummy tissues," in *2013 IEEE International Conference on Robotics and Biomimetics (ROBIO)*. Shenzhen, China: IEEE, Dec. 2013, pp. 1450–1455.

[20] Frauziols, F. *et al.*"*In Vivo* Identification of the Passive Mechanical Properties of Deep Soft Tissues in the Human Leg: *In vivo* Identification of Passive Mechanical Properties of Leg Soft Tissues," *Strain*, vol. 52, no. 5, pp. 400–411, Oct. 2016.